Final Report

JADETHEWEIMARANER

Abstract:

This report discusses the design, fabrication, measurement and analysis of six unbalanced Mach-Zehnder interferometers. The path length differences between the arms in these interferometers ranged from 100µm to 489.2 µm. All interferometers used 220 x 500 nm waveguides. Fabrication was performed using electron beam lithography at the University of Washington. The transmission thru these interferometers were then measured with a custom setup at the University of British Columbia. Transmission data from the interferometers was then used to infer the group index of the waveguide by fitting the empirical data with a theoretical model for the interferometer. These empirically-derived group index and free spectral range values were then compared to simulations performed with Lumerical Mode. A corner analysis was performed to determine if the empirically-derived values for group index and free spectral range were within the expected range due to manufacturing variability. The measured group index and free spectral range agreed well with simulations.

1. Introduction

The following report describes the design, modeling, fabrication, and testing of interferometric photonic integrated circuits for Silicon Photonics Design, Fabrication, and Data Analysis – a course offered online by the University of British Columbia and edX.org. The objective of this design is to develop several interferometer circuits that can be used to assess the group index of the silicon-based waveguide.

The following report starts with a discussion of theory relevant to the interferometric design, with a particular emphasis on strip waveguides and the interferometer transfer function. Initial simulations of the waveguide were performed with Lumerical Mode to estimate the effective and group indices as a function of wavelength. These indices were then uses to estimate the theoretical transmission and free spectral range of an unbalanced Mach-Zehnder interferometer. A series of interferometers with different path differences were then simulated using Lumerical Interconnect. The simulated transmission versus wavelength was then used to estimate the free spectral range and group index of the waveguide used in the interferometer.

The Fabrication, Analysis, and Conclusion portions of the report will be completed later.

2. Theory

Photonic integrated circuits can be built into a variety of materials. Silicon is often chosen due to the advanced fabrication capabilities developed by the electronics industry over many decades.

The Waveguide

One of the key components of a photonic integrated circuit is the waveguide – a microscopic channel that guides light within the silicon wafer. At the most fundamental level, a waveguide consists of a region with higher refractive index surrounded by a region of lower refractive index. This structure allows light to propagate within the chip along prescribed paths.

Silicon photonic designers often work with two types of waveguides, as illustrated in Figure 1. Strip waveguides generally consist of a rectangular, high-index silicon region surrounded by a lower-index material such as silicon dioxide or air. The rib waveguide has a slightly modified

structure and is often used to interface with electrical devices. The proposed interferometer designs described in this report use the strip waveguide.
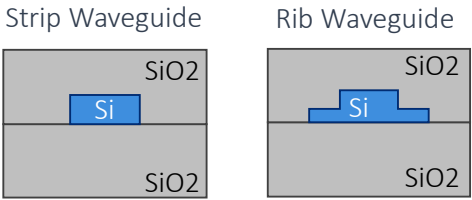

Figure 1. The two waveguide types often used in silicon-based photonic integrated circuits.

A waveguide can support different modes of propagation depending on the waveguide size, shape, and the refractive indices of the associated materials. Figure 2 shows an example of how the spatial distribution of the electric field intensity varies between the 1st TE and TM modes of a 220 nm by 500 nm waveguide. These field intensities were simulated with Lumerical MODE.
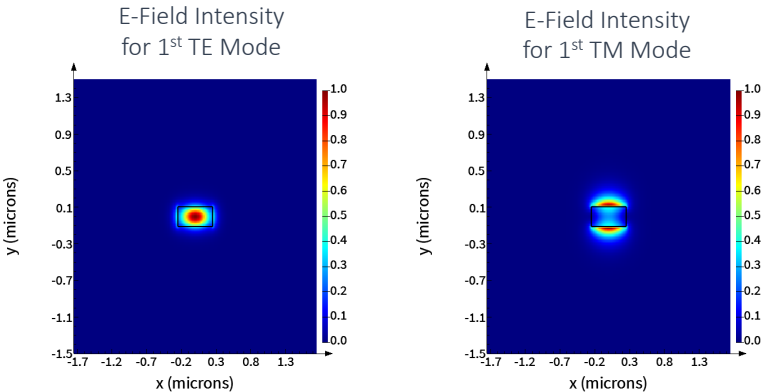

Figure 2. Example of two modes supported by a 220 x 500nm waveguide.

Each mode has unique propagation characteristics such as the effective refractive index, group index, and polarization state. These characteristics for a 220x500nm waveguide are summarized in Figure 3. Note that the first mode is primarily TE polarized, while the second mode is primarily TM polarized. Also, the TE mode is confined more to the waveguide, so it has a higher effective index compared to the TM mode that is confined less to the waveguide.

mode #	effective index	wavelength (µm)	loss (dB/cm)	group index	TE polarization fraction (Ex)	waveguide TE/TM fraction (%)	effective area (µm^2)
1	2.443532+1.246491e-09i	1.55	0.00043889	4.194174+2.661567e-09i	98	76.25 / 81.96	0.190804
2	1.773220+8.620956e-10i	1.55	0.00030354	3.758308+4.314716e-09i	4	68.48 / 88.84	0.356272

Figure 3. Propagation characteristics of the first two modes of a 220x500nm waveguide at 1550nm.

The Mach-Zehnder Interferometer

In this report, a device known as a Mach-Zehnder interferometer is designed and fabricated to test the underlying properties of the waveguide, namely the effective index and group index.

The basic schematics of a balanced and unbalanced Mach-Zehnder interferometer are illustrated in Figure 4. In the balanced Mach-Zehnder interferometer, the input light is split into two paths of equal lengths and then re-combined into the final output waveguide. There are different elements that can be used for the splitter and combiner elements. In the unbalanced

Mach-Zehnder interferometer, the input is split into two paths of unequal length. At the output, the two paths interfere resulting in an output intensity that varies depending on the difference in the waveguides, namely differences in their effective indices and their lengths.
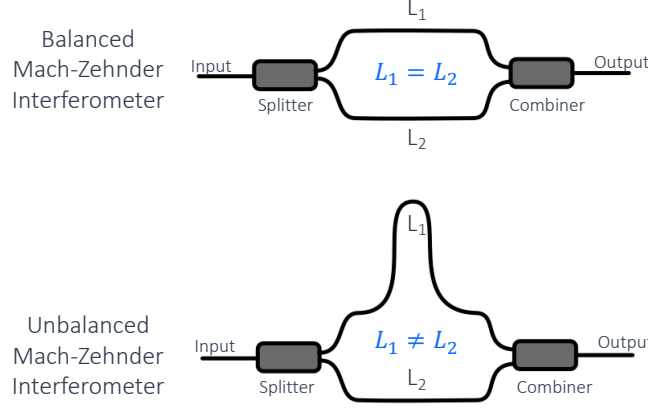

Figure 4. The balanced and unbalanced Mach-Zehnder interferometers.

An unbalanced Mach-Zehnder interferometer was designed, modeled, and fabricated. This Mach-Zehnder interferometer has identical waveguides but with differing lengths. The output intensity for this unbalanced Mach-Zehnder interferometer is given by the following equations

$$I_0 = \frac{I_i}{2}[1 + \cos(\beta \cdot \Delta L)] \text{ and } \beta = \frac{2\pi n_{eff}}{\lambda}$$

Where I_i is the input intensity, β is the propagation constant of the light, n_{eff} is the effective index of the waveguide, λ is the wavelength, and ΔL is the difference in path lengths between the two waveguides.

If the wavelength of the laser is varied, the output of the unbalanced interferometer can constructively or destructively interfere. Constructive interference occurs when the product of the propagation constant and the path length difference equal an integer multiple of 2π, that is $\beta \cdot \Delta L = 2\pi m$. Destructive interference occurs when the product obeys the equation $\beta \cdot \Delta L = \pi(1 + 2m)$. This periodicity of constructive and destructive interference as a function of the input wavelength is a measure called the free spectral range and is given by the following equation

$$FSR = \frac{\lambda^2}{\Delta L \cdot n_g}$$

Where λ is the wavelength, ΔL is the difference in path lengths between the two waveguides, and n_g is the group index defined as

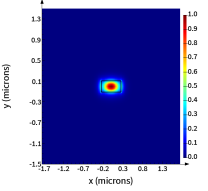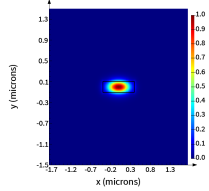$$n_g = n - \lambda\frac{dn}{d\lambda}$$

After fabrication, the free spectral range will be measured with an optical network analyzer. This measured value of the FSR was used to estimate the group index for the waveguide.

3. Modeling and Simulation

Waveguide Simulation

The initial simulations evaluated the first TE mode for two waveguides with different widths. The results of these two simulations are included in Table 1. A wavelength sweep was also included in the simulations to extract the effective index and group index at different wavelengths. A MATLAB script was then used to develop a compact model of the effective index as a function of wavelength. The effective index increases for larger waveguide widths. This occurs because more of the mode propagates in the waveguide and thus has a larger effective index since the waveguide refractive index is larger than the oxide refractive index.

Table 1. Summary of waveguide simulations.

	Waveguide 1	Waveguide 2
Height (nm)	220	220
Width (nm)	500	800
Simulated First TE Mode		
TE Polarization Fraction (%)	98%	100%
Compact Model of Effective Index	$n_{eff} = 2.44 - 1.129 * (\lambda - 1.55) - 0.041 * (\lambda - 1.55)^2$	$n_{eff} = 2.69 - 0.79 * (\lambda - 1.55) + 0.05 * (\lambda - 1.55)^2$

The effective index versus wavelength for the two waveguides is included in Figure 5. The circles are the simulated estimates for the effective index. The lines are the compact model for each waveguide.
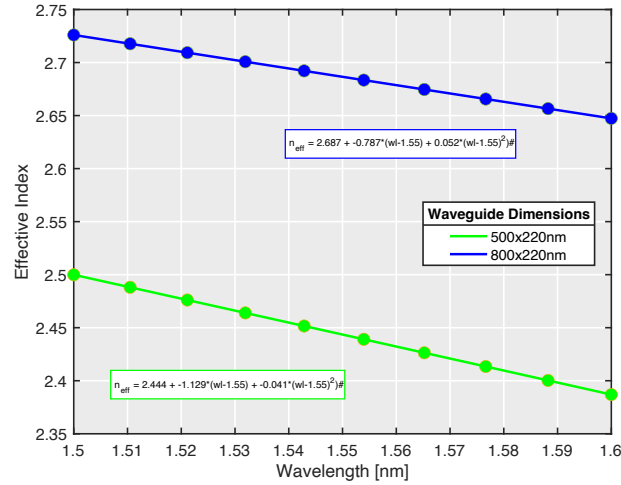

Figure 5. Simulated effective indices versus wavelength for the two waveguides.

The group index versus wavelength for the two waveguides is included in Figure 6. The circles indicate the simulated estimates for the group index at 10 distinct wavelengths between 1500 nm and 1600 nm.
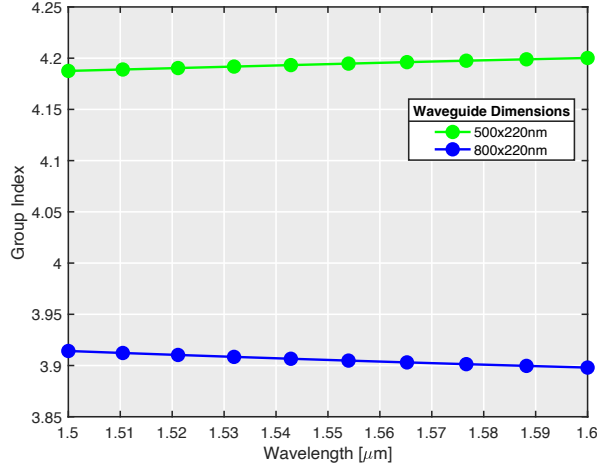

Figure 6. Simulated group indices versus wavelength for the two waveguides

Interferometer Performance Based on Waveguide Simulations

As described in the theory section of the report, the imbalanced Mach-Zehnder interferometer has the following transfer function assuming identical waveguides with differing lengths:

$$I_o = \frac{I_i}{2}[1 + \cos(\beta \Delta L)]$$

With the waveguide simulations, the compact model for the effective index can be used to estimate the propagation constant as a function of wavelength. The propagation constants for the two waveguides are updated to use the compact models fitted from the waveguide simulations, that is,

$$\beta = \frac{2\pi n_{eff}}{\lambda} = \frac{2\pi(2.44 - 1.129\lambda_{[\mu m]} - 0.041\lambda^2_{[\mu m]})}{\lambda}$$

$$\beta = \frac{2\pi n_{eff}}{\lambda} = \frac{2\pi(2.69 - 0.787\lambda_{[\mu m]} + 0.052\lambda^2_{[\mu m]})}{\lambda}$$

Figure 7 are the estimates for the interferometer transmission based on this theoretical transfer function and the compact models of the two simulated waveguides. The 500x220nm waveguide (green) has a smaller FSR than the 800x220nm waveguide (blue) as expected since the 800x220nm has a lower group index. The top plot shows the transmission in percent of the input intensity. The bottom plot shows the transmission in dB from the input intensity. The transfer function describes the ideal interferometer so loss and coupling efficiencies of real-world components are not included in these plots but will be the evaluated in simulations later in the report.
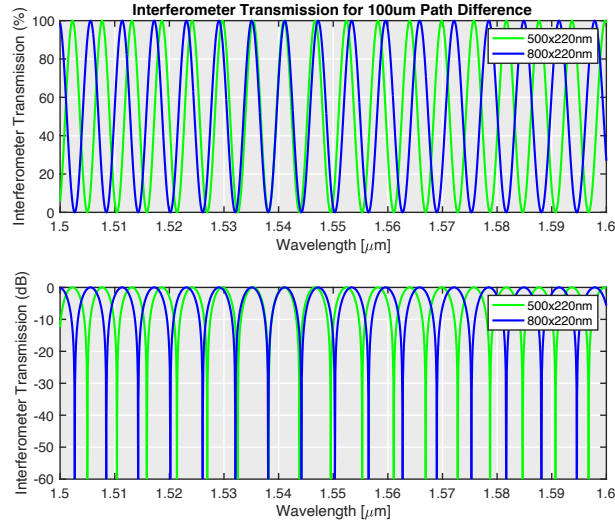
Figure 7. Interferometer transmission as a function of wavelength for $\Delta L = 100\mu m$. Green is the interferometer transmission for the 500x220nm waveguide. Blue is the interferometer transmission for the 800x220nm waveguide.

Similarly, the estimated free spectral range can be updated with the simulated group indices for the two waveguides. A series of six Mach-Zehnder interferometers were designed using the 500um wide waveguide. Table 2 provides the estimated FSR for six Mach-Zehnder interferometers with different combinations of path length differences.

Table 2. Free spectral range calculations based on waveguide simulations.

Design	Path Length Difference	Waveguide Width	*Calculated FSR*
A1	100 μm	0.500 μm	5.73 nm
A2	200 μm	0.500 μm	2.86 nm
A3	300 μm	0.500 μm	1.91 nm
A4	400 μm	0.500 μm	1.43 nm
B1	300 μm	0.500 μm	1.91 nm
B2	489.2 μm	0.500 μm	1.16 nm

Interferometer Simulations

Each design was modeled in Lumerical Interconnect using the SiEPIC Ebeam design kit. Figure 8 thru Figure 13 show both the interferometer layout and the corresponding transmission spectrum. Note that each interferometer uses the TE1550 grating coupler, the waveguide, and the Y-branch coupler from the SiEPIC Ebeam design kit. The length and width of the waveguide was varied between the six interferometer designs.
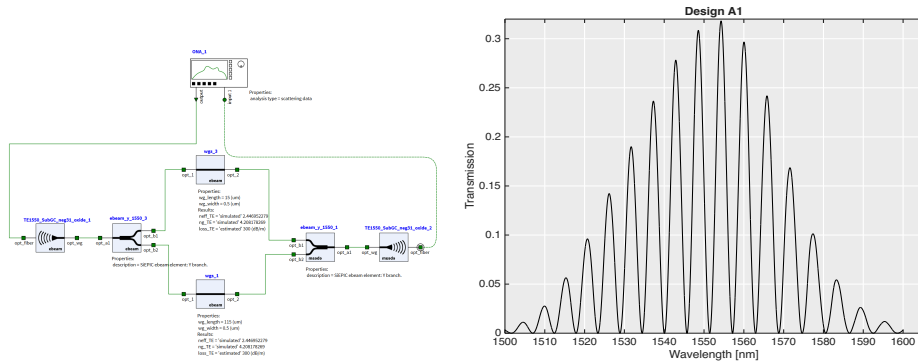
Figure 8. Lumerical Interconnect simulation of Design A1 (path difference of 100um and waveguide width = 500nm)
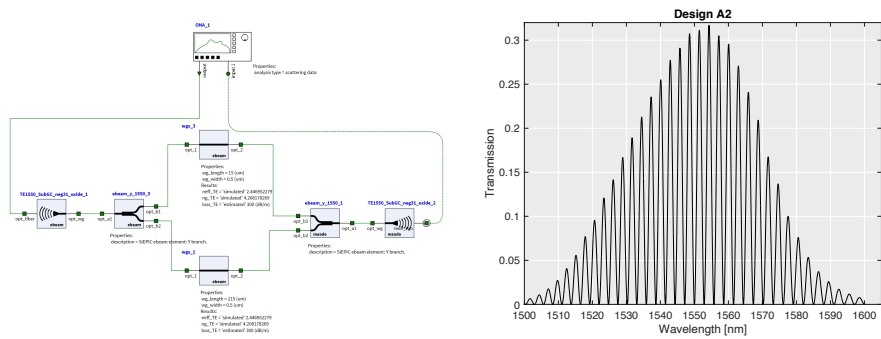

Figure 9. Lumerical Interconnect simulation of Design A2 (path difference of 200um and waveguide width = 500nm)
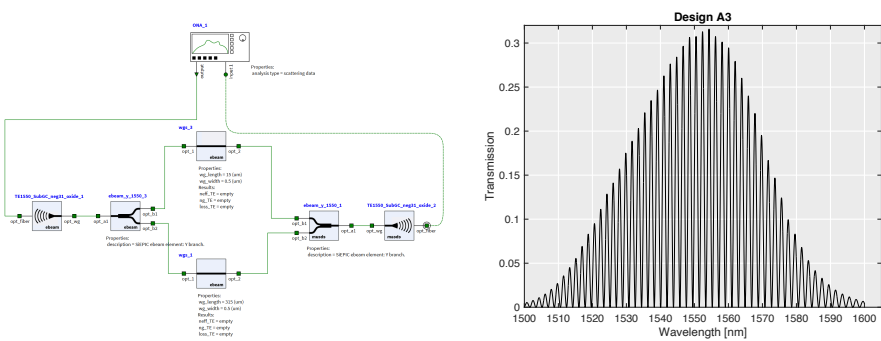

Figure 10. Lumerical Interconnect simulation of Design A3 (path difference of 300um and waveguide width = 500nm)
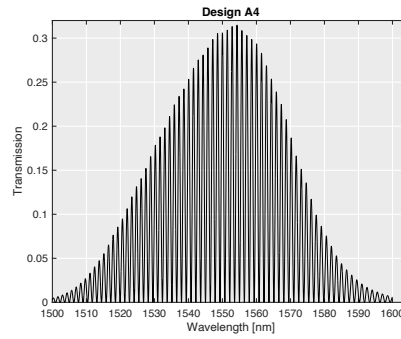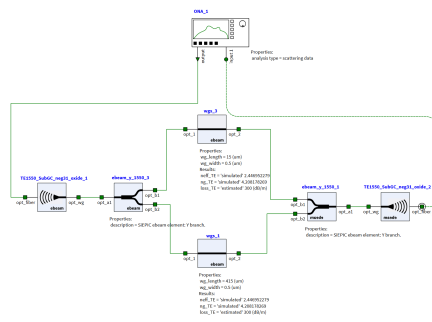
Figure 11. Lumerical Interconnect simulation of Design A4 (path difference of 400um and waveguide width = 500nm)
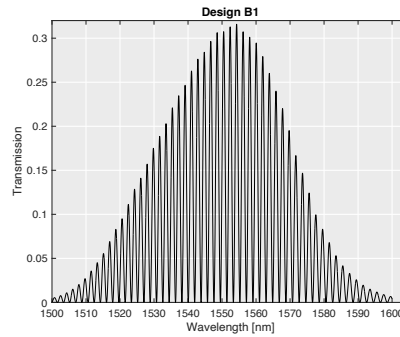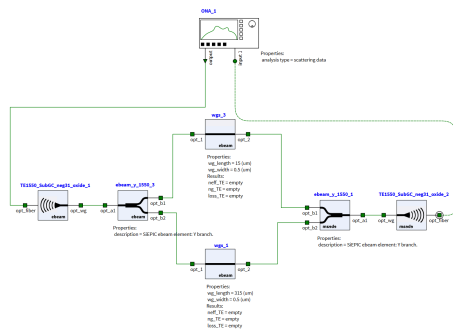

Figure 12. Lumerical Interconnect simulation of Design B1 (path difference of 300um and waveguide width = 500nm)
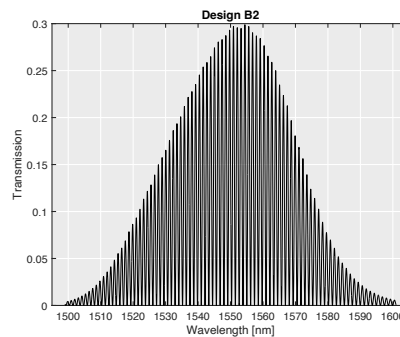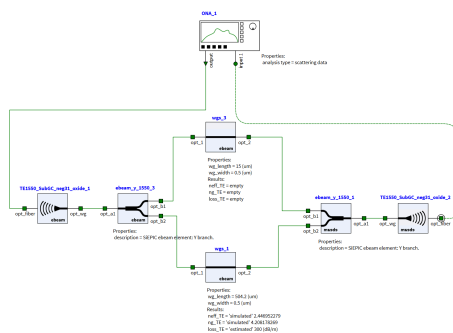

Figure 13. Lumerical Interconnect simulation of Design B2 (path difference of 489.2um and waveguide width = 500nm)

4. Fabrication

The device layout was performed with the KLayout software and merged with other designs from the class into a master layout file. The layout for the six interferometer circuits is shown in Figure 14. Since there was some extra space in the allotted space, a few additional circuits were integrated for de-embedding (i.e. monitoring transmission of grating couplers and splitters) as well as a micro-ring resonator. This report focuses on the analysis of the unbalanced Mach-Zehnder interferometers; the analysis of these extra circuits are not included.
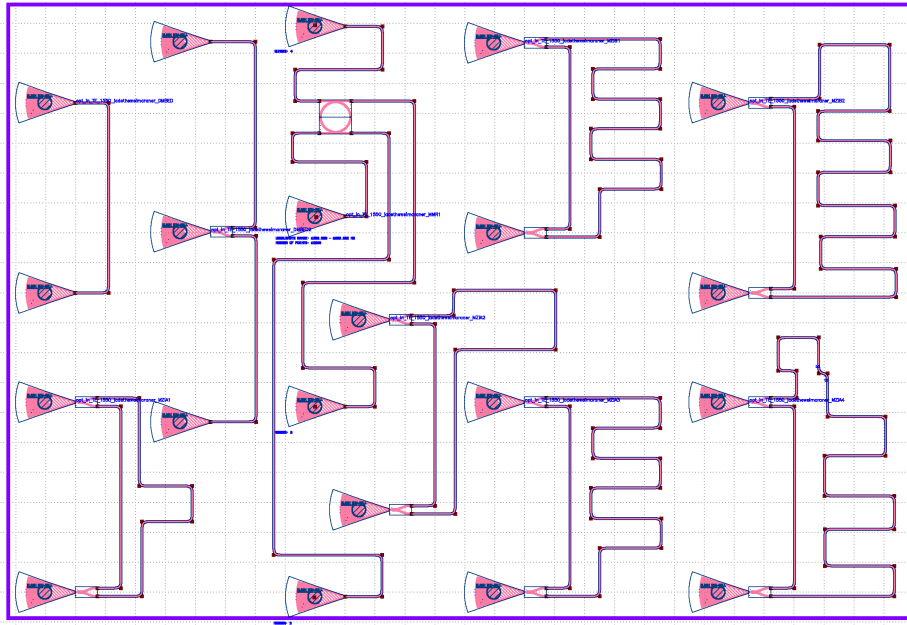

Figure 14. The layout of the fabricated circuits discussed later in this report.

The devices were fabricated using 100 keV Electron Beam Lithography [1]. The fabrication used silicon-on-insulator wafer with 220 nm thick silicon on 3 µm thick silicon dioxide. The substrates were 25 mm squares diced from 150 mm wafers. After a solvent rinse and hot-plate dehydration bake, hydrogen silsesquioxane resist (HSQ, Dow-Corning XP-1541-006) was spin-coated at 4000 rpm, then hotplate baked at 80 °C for 4 minutes. Electron beam lithography was performed using a JEOL JBX-6300FS system operated at 100 keV energy, 8 nA beam current, and 500 µm exposure field size. The machine grid used for shape placement was 1 nm, while the beam stepping grid, the spacing between dwell points during the shape writing, was 6 nm. An exposure dose of 2800 µC/cm2 was used. The resist was developed by immersion in 25% tetramethylammonium hydroxide for 4 minutes, followed by a flowing deionized water rinse for 60 s, an isopropanol rinse for 10 s, and then blown dry with nitrogen. The silicon was removed from unexposed areas using inductively coupled plasma etching in an Oxford Plasmalab System 100, with a chlorine gas flow of 20 sccm, pressure of 12 mT, ICP power of 800 W, bias power of 40 W, and a platen temperature of 20 °C, resulting in a bias voltage of 185 V. During etching, chips were mounted on a 100 mm silicon carrier wafer using perfluoropolyether vacuum oil. Cladding oxide was deposited using plasma enhanced chemical vapor deposition (PECVD) in an Oxford Plasmalab System 100 with a silane (SiH4) flow of 13.0 sccm, nitrous oxide (N2O) flow of 1000.0 sccm, high-purity nitrogen (N2) flow of 500.0 sccm, pressure at 1400mT, high-frequency RF power of 120W, and a platen temperature of

350C. During deposition, chips rest directly on a silicon carrier wafer and are buffered by silicon pieces on all sides to aid uniformity.

5. Experimental Data

To characterize the devices, a custom-built automated test setup [2, 6] with automated control software written in Python was used [3]. An Agilent 81600B tunable laser was used as the input source and Agilent 81635A optical power sensors as the output detectors. The wavelength was swept from 1500 to 1600 nm in 10 pm steps. A polarization maintaining (PM) fibre was used to maintain the polarization state of the light, to couple the TE polarization into the grating couplers [4]. A 90º rotation was used to inject light into the TM grating couplers [4]. A polarization maintaining fibre array was used to couple light in/out of the chip [5].

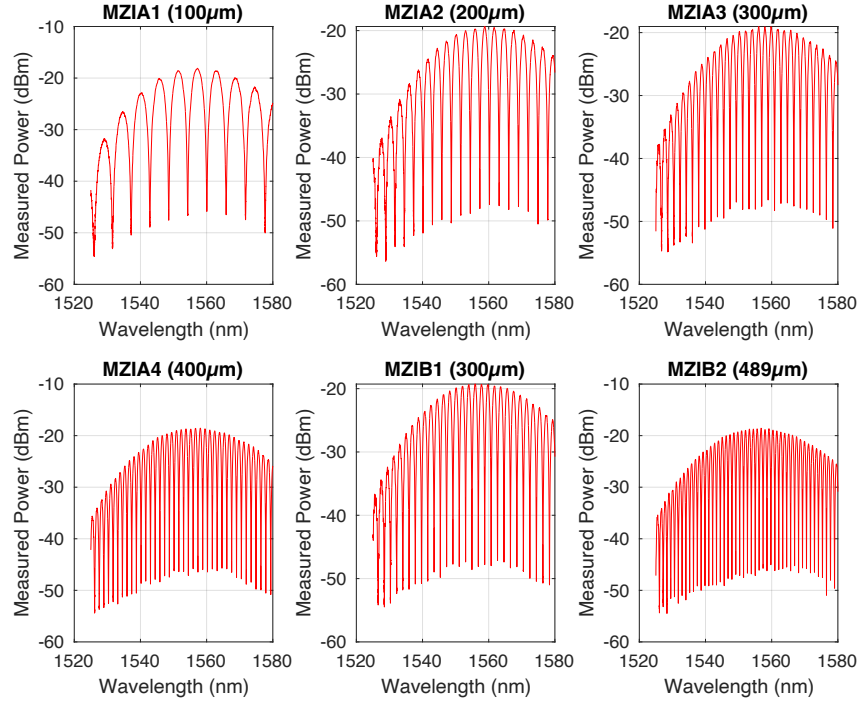The raw measurements for the six unbalanced Mach-Zehnder interferometers are included in Figure 15.

Figure 15. Raw transmission data collected from the six unbalanced Mach-Zehnder interferometers.

6. Analysis

Determining Group Index from Interferometer Transmission Data

The transmission through each interferometer is measured as a function of wavelength. An example of this measurement is included as the blue curve in Figure 16. The wavelength dependent attenuation of the transmission measurements is primarily due to wavelength dependence of the grating coupler. This wavelength dependence is removed from the data by fitting a 5th order polynomial to the attenuation data. This polynomial is then subtracted from the data and the result is renormalized. The result of this process is shown as the red curve in Figure 16.
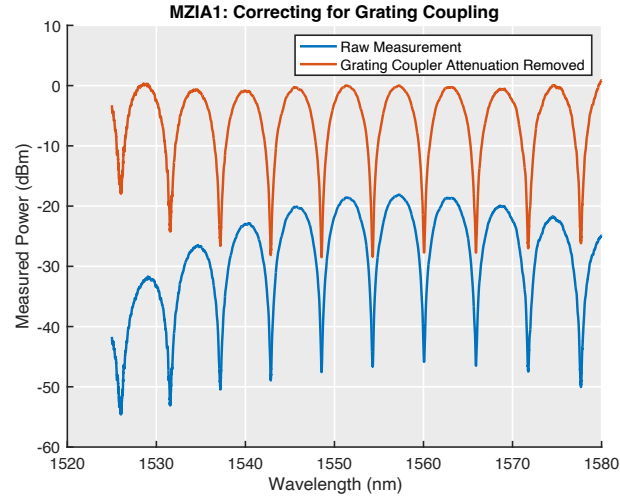
Figure 16. Correcting the wavelength-dependent attenuation of the grating coupler.

The next process is fitting this normalized transmission with the theoretical transmission of an unbalanced Mach-Zehnder interferometer. To perform this fitting operation, a set of initial parameters need to be estimated from the measured data. The free spectral range versus wavelength is determined using the minimums of the transmission data (red circles), as illustrated in Figure 17.
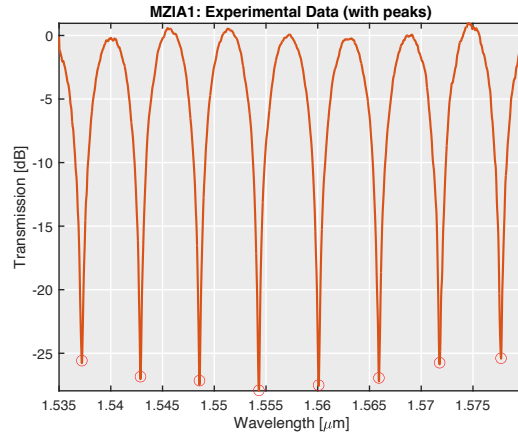

Figure 17. Finding the minima of the interferometer transmission for calculating the FSR.

The measured free spectral range (Figure 18) is then converted to group index using the known path length mismatch and the wavelength. The first three terms in a Taylor expansion for the waveguide effective index are estimated using this measured data. The first term is estimated based on the path length, the second term is estimated by the average group index, and the third term is estimated based on the slop of the group index relative to the wavelength.
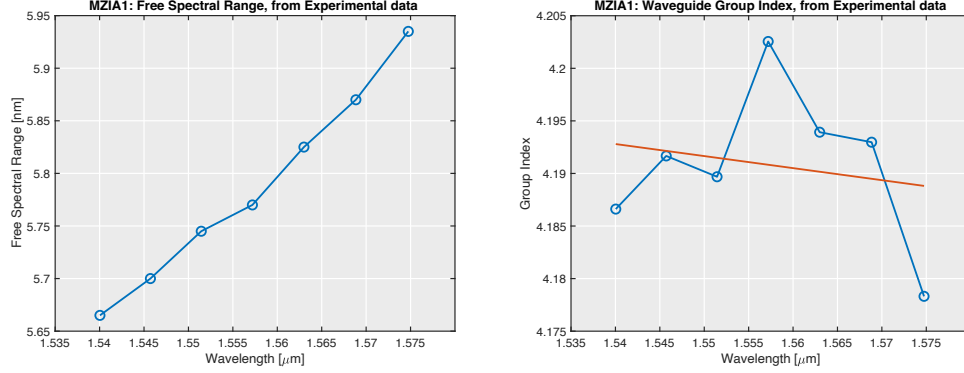
Figure 18. Calculating the free spectral range from the interferometer transmission measurements and using FSR to infer the initial conditions for the fitting operation.

These measured initial values provide a good fit to the data as shown in Figure 19. A least-squares curvefitting algorithm tunes these parameters (three terms in Taylor expansion for waveguide effective index, the waveguide propagation loss, and a DC offset term). The MZI model before and after fitting are shown in Figure 19.
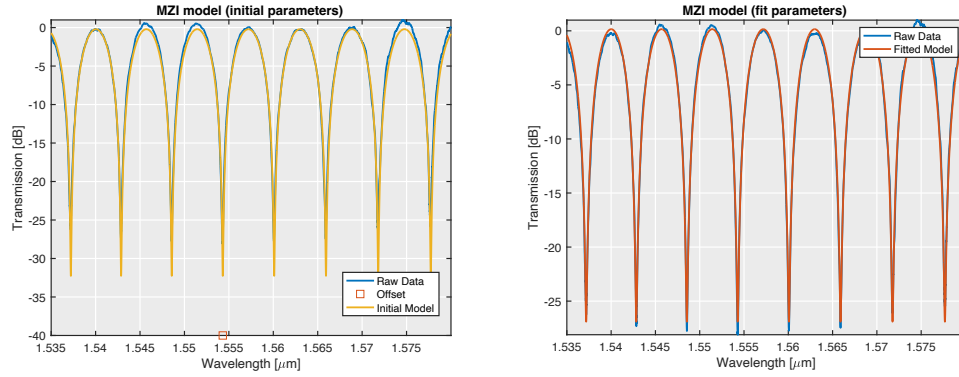

Figure 19. The interferometer model before and after the least squares curve fit.

This process was repeated for all six interferometer measurements. The measured FSR, group index, and dispersion for the six interferometers are included in Table 3. Note that the measured group indices agree well with those simulated from the waveguides (Figure 6).

Table 3. Free spectral range and group index calculations based on simulated interferometer transmission measurements.

Design	Path Length Difference	Waveguide Width	Theoretical FSR (at 1550nm)	Measured FSR (at 1550nm)	Simulated n_g (at 1550nm)	Measured n_g from (at 1550nm)
A1	100 μm	0.500 μm	5.73 nm	5.739 nm	4.19	4.187
A2	200 μm	0.500 μm	2.86 nm	2.872 nm	4.19	4.183
A3	300 μm	0.500 μm	1.91 nm	1.914 nm	4.19	4.183
A4	400 μm	0.500 μm	1.43 nm	1.436 nm	4.19	4.182
B1	300 μm	0.500 μm	1.91 nm	1.914 nm	4.19	4.183
B2	489.2 μm	0.500 μm	1.16 nm	1.174 nm	4.19	4.182

Manufacturing Variability - Corner Analysis

As with all fabrication processes, electron beam lithography introduces some variability into the fabricated structures. To estimate this variability and the impact on our measurements, a corner analysis was performed to estimate how the group index varies due to slight changes in the thickness and width of the nominal 220nm thick and 500nm wide waveguide. In this corner analysis, we assumed the waveguide thickness could vary from 215.3 to 223.1nm and the waveguide width could vary from 470 to 515nm. Four different waveguides were simulated representing the bounds of what would be expected from the electron beam lithography fabrication, as summarized in Table 4. These simulations provided the group index would most likely range from 4.175 to 4.254.

Table 4. The waveguides analyzed in the variability corner analysis

Waveguide	Thickness	Width
A	215.3 nm	470 nm
B	215.3 nm	515 nm
C	223.1 nm	470 nm
D	223.1 nm	515 nm

Table 5 compares the measured values of FSR and group index compared to the range expected from the corner analysis. These results show that the measured results fall within the range expected due to manufacturing variability.

Table 5. Comparison of measured FSR and group index values compared to simulated corner analysis.

Design	Path Length Difference	Minimum FSR from corner analysis	Maximum FSR from corner analysis	FSR from Data (at 1550nm)	Minimum n_g from corner analysis (at 1550nm)	Maximum n_g from corner analysis (at 1550nm)	n_g from Data (at 1550nm)
A1	100 μm	5.648 nm	5.754 nm	5.739 nm	4.175	4.254	4.187
A2	200 μm	2.824 nm	2.877 nm	2.872 nm	4.175	4.254	4.183
A3	300 μm	1.883 nm	1.918 nm	1.914 nm	4.175	4.254	4.183
A4	400 μm	1.412 nm	1.439 nm	1.436 nm	4.175	4.254	4.182
B1	300 μm	1.883 nm	1.918 nm	1.914 nm	4.175	4.254	4.183
B2	489.2 μm	1.154 nm	1.176 nm	1.174 nm	4.175	4.254	4.182

7. Conclusions

The goal of this effort was to learn how to design, model, fabricate, measure, and evaluate unbalanced Mach Zehnder interferometers. Measurements of the interferometer transmission were used to estimate the real group index of the silicon waveguide and the free spectral range of each interferometer. These empirically-derived group indices agreed quite well with those predicted using simulations in Lumerical Mode. Slight differences between the simulated and empirical group indices and free spectral ranges could be explained with expected manufacturing variability of the waveguide. This effort demonstrates the fidelity of modern simulation tools for predicting the real-world optical performance of silicon photonics devices. However, the effort also showed the importance of considering how normal manufacturing

variability can lead to some uncertainty in the performance of the fabricated device. Corner or Monte Carlo analyses can be used to help quantify the range of performance that can be expected from a fabricated device.

8. Acknowledgements

9. References

[1] R. J. Bojko, J. Li, L. He, T. Baehr-Jones, M. Hochberg, and Y. Aida, "Electron beam lithography writing strategies for low loss, high confinement silicon optical waveguides," J. Vacuum Sci. Technol. B 29, 06F309 (2011)

[2] Lukas Chrostowski, Michael Hochberg, chapter 12 in "Silicon Photonics Design: From Devices to Systems", Cambridge University Press, 2015

[3] http://siepic.ubc.ca/probestation, using Python code developed by Michael Caverley.

[4] Yun Wang, Xu Wang, Jonas Flueckiger, Han Yun, Wei Shi, Richard Bojko, Nicolas A. F. Jaeger, Lukas Chrostowski, "Focusing sub-wavelength grating couplers with low back reflections for rapid prototyping of silicon photonic circuits", Optics Express Vol. 22, Issue 17, pp. 20652-20662 (2014) doi: 10.1364/OE.22.020652

[5] www.plcconnections.com, PLC Connections, Columbus OH, USA.

[6] http://mapleleafphotonics.com, Maple Leaf Photonics, Seattle WA, USA.